TECHNISCHE MECHANIK, 32, 2-5, (2012), 321-332
submitted: September 30, 2011

Simulation of Non-Isothermal Mechanical Tests on a Single Crystal Nickel-Basis Superalloy

V. Kindrachuk, B. Fedelich

An extension of the constitutive viscoplastic model of Meric and Cailletaud is presented. The new model accounts for coupling of plasticity and viscoplasticity to describe the rate dependence at low and moderate temperatures. The model contains two boundaries: an elastic one and a viscoplastic one. Between the boundaries, the only contribution to yielding is the rate dependent viscoplastic mechanism. Once the viscoplastic boundary is reached, an additional rate independent flow mechanism becomes active. However, the extended model is not able to predict properly both creep and long-term relaxation tests simultaneously. Therefore, a deformation-induced softening is assumed, which is supposed to mainly affect static recovery.

The model has been calibrated with the mechanical tests on a single crystal nickel-basis superalloy. The uniaxial tests have been carried out in the temperature interval 600°C – 1100°C in [001], [011] and [111] specimens. The predicted creep, relaxation and non-isothermal cyclic tests exhibit reasonable agreement with the experimental observations.

1 Introduction

Turbine blades in aero engines experience thermo-mechanical loadings over temperatures ranging from room temperature up to 1100°C. Hence, constitutive laws should be able to represent the mechanical behavior of the blade alloy in the whole temperature range of operation. In the case of single crystal superalloys, an intricate dependence of the behavior on the orientation has also to be taken care of.

While in the last two decades a large number of constitutive models for single crystals of superalloys have been proposed, most applications are concerned with a restricted temperature range and studies for a large temperature range are scarce. In addition, blades undergo a complex mechanical loading, including creep, cyclic straining but also the relaxation of thermal stresses. However, many studies are restricted to special loading types. In particular, an important number of models are focused on pure creep (see e.g., Glatzel and Brehm, 1999; MacLachlan, Wright et al., 2001). Only a few papers consider applications to both creep and fatigue (e.g., Meric, Poubanne et al., 1991; Li and Smith, 1998; Staroselsky and Cassenti, 2011). Applications of the constitutive models to long-term stress relaxation are even scarcer. In summary, there is a need for verification of constitutive models for single crystal of superalloys in a broad range of loading situations including long-term stress relaxation in addition to creep, cyclic straining and thermo-mechanical loading in a large range of temperatures.

This paper presents an extension of the model developed by Méric, Poubanne and Cailletaud (1991) to better simultaneously describe creep, fatigue, cyclic relaxation and long-term relaxation in a representative range of temperatures for the operation of turbine blades. The model has been applied to a typical single crystal superalloy, which is widely used for aero engine applications. A similar approach has recently been proposed for polycrystalline superalloys by Becker and Hackenberg (2011).

2 Mechanical Tests

In order to investigate the plastic and the viscous response of the superalloy, a test program has been carried out at constant temperatures from 600°C to 1100°C. In this paper we present the results of two types of uniaxial isothermal tests: constant load creep tests and strain-controlled tests. The last one consists of two blocks. The first one is a cyclic push-pull sequence at a constant strain rate of 10^{-3} s^{-1}, with increasing strain amplitude as shown in Figure 1. The second block is a constant strain with the hold time of 1 h (for the test at 600°C), 50 h (800°C and 950°C) and 20 h (1100°C). The cyclic straining enables us to identify the hardening behavior of the

superalloy. The beginning of the stress relaxation (second block) is mostly related to the relaxation of the viscous overstress, whereas the long-term relaxation and creep are controlled by the balance between hardening and thermal recovery. Thus, this testing program allows us to investigate the major effects of high temperature superalloy mechanical behavior.

Experimental results from [001] and [111] specimens only were used for the purpose of the model calibration. The results observed in [011] orientation were used for validation only. The thermo-mechanical tests were carried out in the temperature range from 600°C to 1100°C under out of phase 135° and 180° conditions.

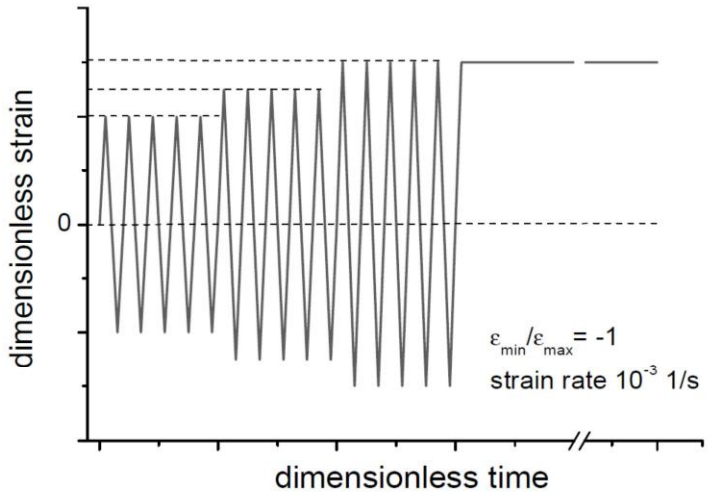

Figure 1: Strain-controlled test

3 Constitutive Model for Single Crystals

3.1 Crystallographic Viscoplastic Model of Cailletaud

The constitutive model introduced by Méric, Poubanne and Cailletaud (1991), in the following simply referred to as the Cailletaud model, can be regarded as a one-dimensional formulation of the Chaboche model (2008) on each slip system. The viscoplastic strain rate $\dot{\boldsymbol{\varepsilon}}^{vp}$ is the sum over shear strain rates $\dot{\gamma}_g$ on all slip systems

$$\dot{\boldsymbol{\varepsilon}}^{vp} = \sum_{g \in G} \dot{\gamma}_g \cdot \boldsymbol{\mu}_g, \tag{1}$$

where G is the set of possible slip systems and $\boldsymbol{\mu}_g$ denotes the orientation tensor corresponding to the slip system g. We consider face-centered cubic single crystals and account for twelve octahedral and six cubic slip systems. Thus G consists of a total of 18 slip systems. The stress tensor is determined by the linear relation

$$\boldsymbol{\sigma} = \mathbf{C} : \left(\boldsymbol{\varepsilon} - \boldsymbol{\varepsilon}^{vp} \right), \tag{2}$$

where $\boldsymbol{\varepsilon}$ is the total strain and $\mathbf{C}$ represents the fourth-order elasticity tensor.

Now we consider the viscoplastic flow rule. The viscoplastic shear strain rate (denoted by the superscript "*vp*") is expressed as a function of the overstress ϕ_g according to the Norton's law

$$\dot{\gamma}_g^{vp} = \left\langle \frac{\phi_g}{K_g} \right\rangle^{n_g} \cdot \operatorname{sign}\left(\tau_g - x_g \right). \tag{3}$$

Here $\langle x \rangle := (x + |x|)/2$ denotes the McCauley brackets and K_g and n_g are slip system dependent model parameters. In the following, slip system dependent model parameters will be assumed to take different values for octahedral $(g \in [1,12])$ and cubic $(g \in [13,18])$ slip systems. The overstress

$$\phi_g = |\tau_g - x_g| - R_{0g} - r_g \tag{4}$$

is a function of the resolved shear stress $\tau_g = \boldsymbol{\sigma} : \boldsymbol{\mu}_g$, the back stress x_g and the isotropic hardening contribution r_g to the yield stress R_{0g}. Equation $\phi_g = 0$ defines the boundary of elasticity domain. The evolution of kinematic hardening follows from the Armstrong and Frederick equation (Armstrong and Frederick, 2007). The growth of the back-stress x_g is compensated by the dynamic (DR_g) and static (SR_g) recovery terms

$$\begin{aligned} x_g &= c_g \alpha_g, \\ \dot{\alpha}_g &= \dot{\gamma}_g^{vp} - \dot{\omega}_g \cdot DR_g - SR_g. \end{aligned} \tag{5}$$

Here α_g is a strain-like kinematic internal variable associated to the back stress; $\dot{\omega}_g = |\dot{\gamma}_g^{vp}|$ denotes the accumulated shear strain rate, c_g is a material parameter. Both recovery terms are power law functions of α_g, like in the flow rule (3), *i.e.*

$$\begin{aligned} DR_g &= DR_g(\alpha_g) = \left(\frac{\alpha_g}{D_g} \right)^{d_g}, \\ SR_g &= \operatorname{sign}(x_g) \cdot \left(\frac{|x_g|}{M_g} \right)^{m_g} = c_g^{m_g} \cdot \operatorname{sign}(\alpha_g) \cdot \left(\frac{|\alpha_g|}{M_g} \right)^{m_g}. \end{aligned} \tag{6}$$

The Cailletaud model considers an interaction between slip systems at the level of the isotropic hardening. The interaction is expressed by the interaction matrix H_{gi} (influence of the slip system „i“ on the system “g”). Thus the isotropic internal variable accounting for the interaction is given as

$$r_g = Q_g \cdot \sum_{i \in G} H_{gi} \cdot \left(1 - \exp(-b_i \omega_i)\right). \tag{7}$$

In case of self-hardening, the interaction matrix reduces to the identity matrix.

3.2 Extension of the Model of Cailletaud for the Rate-Independent Behavior

Viscoplastic constitutive models can properly simulate the high-temperature behavior of metals and alloys. However, using viscoplasticity for low or even moderate temperatures can lead to numerical difficulties. This is caused by high Norton's exponents needed in a nearly rate-independent regime. Therefore, a numerically robust model valid over the whole temperature range should incorporate both viscoplastic and plastic behaviors. With this in mind, we assume that the inelastic shear strain rate is the sum of the viscoplastic and plastic contributions

$$\dot{\gamma}_g = \left(\left\langle \frac{\phi_g}{K_g} \right\rangle^{n_g} + \dot{\lambda}_g^p \right) \cdot \operatorname{sign}(\tau_g - x_g) = \dot{\omega}_g \cdot \operatorname{sign}(\tau_g - x_g), \tag{8}$$

where $\dot{\omega}_g$ denotes further the inelastic accumulated shear strain rate

$$\dot{\omega}_g = \left|\dot{\gamma}_g\right| = \left\langle \frac{\phi_g}{K_g} \right\rangle^{n_g} + \dot{\lambda}_g^p = \left|\dot{\gamma}_g^{vp}\right| + \dot{\lambda}_g^p. \tag{9}$$

In contrast to (3), the relation for the inelastic shear strain rate (8) contains the additional term $\dot{\lambda}_g^p$ associated with the rate-independent behavior (denoted by the superscript "p"). The plastic shear strain rate $\dot{\lambda}_g^p$ satisfies the Kuhn-Tucker conditions (Simo and Hughes, 1998)

$$f_g \dot{\lambda}_g^p = 0,\ \dot{\lambda}_g^p \geq 0,\ f_g \leq 0,\ \forall\ g \in G, \tag{10}$$

where the relation $f_g = 0$ bounds the viscoplastic region. We assume identical hardening of the viscoplastic and plastic deformation mechanisms, i.e. the function f_g is given by

$$f_g = \left|\tau_g - x_g\right| - L_{0g} - r_g, \tag{11}$$

in which the width of the viscoplastic region remains constant, that is. $\phi_g - f_g = L_{0g} - R_{0g} = constant \geq 0$.

Using (8) we introduce the inelastic strain rate $\dot{\boldsymbol{\varepsilon}}^{in}$ similar to (1)

$$\dot{\boldsymbol{\varepsilon}}^{in} = \sum_{g \in G} \dot{\gamma}_g \cdot \boldsymbol{\mu}_g = \dot{\boldsymbol{\varepsilon}}^{vp} + \dot{\boldsymbol{\varepsilon}}^{p} \tag{12}$$

where

$$\begin{aligned} \dot{\boldsymbol{\varepsilon}}^{vp} &= \sum_{g \in G} \dot{\gamma}_g^{vp} \cdot \boldsymbol{\mu}_g = \sum_{g \in G} \left\langle \frac{\phi_g}{K_g} \right\rangle^{n_g} \cdot \boldsymbol{\mu}_g \cdot \operatorname{sign}(\tau_g - x_g), \\ \dot{\boldsymbol{\varepsilon}}^{p} &= \sum_{g \in G} \dot{\lambda}_g^{p} \cdot \boldsymbol{\mu}_g \cdot \operatorname{sign}(\tau_g - x_g). \end{aligned} \tag{13}$$

are the viscoplastic and plastic strain rates respectively. The inelastic strain tensor and the stress tensor in (2) are then given by the modified equations

$$\begin{aligned} \boldsymbol{\varepsilon}^{in} &= \boldsymbol{\varepsilon}^{vp} + \boldsymbol{\varepsilon}^{p}, \\ \boldsymbol{\sigma} &= \mathbf{C} : \left(\boldsymbol{\varepsilon} - \boldsymbol{\varepsilon}^{in}\right). \end{aligned} \tag{14}$$

3.3 Modeling of Softening Behavior

It was found that the initial version of the model of Cailletaud is not able to predict properly both creep and long-term relaxation tests simultaneously. An improvement in simulation of relaxation tests results in a worse simulation of creep tests and vice versa. A simulation of stress relaxation in a [001]-orientated sample at 950°C by means of the Cailletaud model is presented in Figure 2 (left). The predicted long-term stress relaxation overestimates the observed stress values, whereas the stationary creep is consistent with the experimental observations (Figure 3, black curves). Note that this creep-relaxation incompatibility also occurs for the tests at 1100°C. In order to improve the model prediction, the influence of flow function on the creep-relaxation behavior was investigated in (Kindrachuk, Fedelich et al., 2010). Particularly, the sinus hyperbolicus flow rule was included in (3) and (6) instead of the power law functions. The sinus hyperbolicus function behaves linearly for small overstresses in contrary to the power law function, which is negligibly smaller. However, no remarkable improvement in overcoming the incapability creep-relaxation could be obtained by this means.

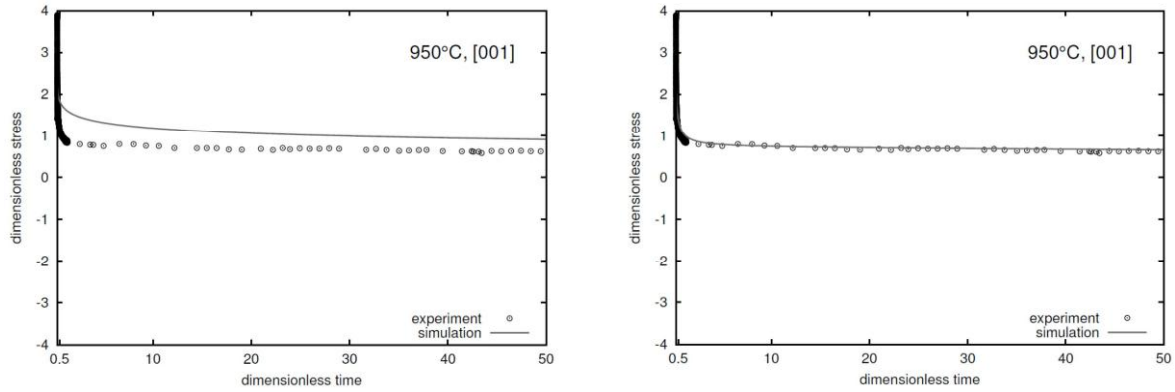

Figure 2: Predicted relaxation curves against experimental data along [001] direction at 950°C. Simulation by the initial (left) and by the modified (right) model of Cailletaud.

In the present paper a type of deformation-induced softening is assumed that only affects static recovery, and thus the long-term behavior, i.e. long-term relaxation and creep. In particular it results in a higher relaxation rate after cyclic straining in comparison to the initial model and can predict creep acceleration as well (beginning of tertiary creep).

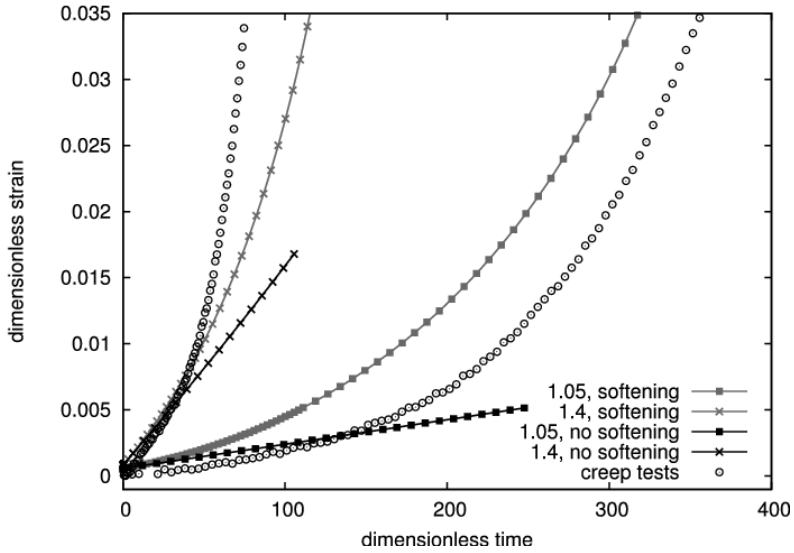

Figure 3: Creep tests along [001] crystallographic direction at 950°C performed at normalized stresses 1.05 and 1.4. The initial Cailletaud model (black curves) predicts stationary creep. The modified model (grey curves) accounts for softening and predicts tertiary creep. The experimental data are plotted with open cycles.

More specifically, we introduce deformation-induced softening by assuming dependence of the static recovery exponent m_g on the accumulated shear

$$SR_g = \text{sign}(x_g)\cdot\left\langle\frac{|x_g|-\tilde{x}_g}{M_g}\right\rangle^{m_g},$$
$$m_g = m_{\infty g}+\left(m_{0g}-m_{\infty g}\right)\cdot\exp(-a_g\omega_g),\ \ m_{0g}\geq m_{\infty g}, \tag{15}$$

where $\tilde{x}_g$ threshold for static recovery. The model parameters m_{0g} and $m_{\infty g}$ characterize the exponent m_g at the beginning of loading and in the long-term respectively; a_g describes the rate of softening. The extended model reduces to the initial model of Cailletaud if $a_g = 0$, then $m_g = m_{0g}$ is a constant. The value of the

threshold $\tilde{x}_g$ for the octahedral slip systems can be easily estimated from a [001] test. Indeed, in the stationary state (denoted by the superscript "*") $\dot{\gamma}_g^{vp}* = 0$, $\dot{x}_g^* = 0$, and hence as follows from (3) and (5), $\phi_g^* = 0$ and $SR_g^* = 0$. Taking the relation for the static recovery (15) and for ϕ_g (4) we obtain

$$\tilde{x}_g = x_g* = \frac{\sigma_{[001]}^*}{\sqrt{6}} - R_{0g}. \tag{16}$$

The value of the threshold $\tilde{x}_g$ for cubic slip systems can be similarly estimated from a relaxation test along the [111] crystallographic direction. The obtained parameters can be used as the start value in an iterative model calibration procedure.

A comparison between the initial Cailletaud model and the extended model in predicting long-term relaxation and creep is represented in Figures 2 and 3. Figure 2 (right) demonstrates the accurate simulation of relaxation by means of the extended model. As seen in Figure 3, creep acceleration (open cycles) takes place at small strains of about 0.005. The initial model (black curves) can only predict secondary creep, whereas the extended model (grey curves) simulates creep acceleration as well. The beginning of the tertiary creep can be associated with several phenomena including rafting, morphology coarsening, cutting of the γ' precipitates and a decrease of the dislocation density in γ/γ' interfaces.

The thermodynamic consistency of the extended model can be easily proven checking the positivity of dissipation. The incremental form of the model has been implemented through the UMAT subroutine in the ABAQUS finite element program. For details concerning the practical aspects of the implementation procedure, the reader is referred to (Kindrachuk and Fedelich, 2011).

3.4 Calibration Strategy

All material parameters are temperature-dependent and have been determined for temperatures in the range 600°C – 1100°C. First of all, the identification procedure is applied to the model parameters for the octahedral slip systems. For this purpose we have only used the tests carried out on the [001] orientated samples, since the cubic slip systems are inactive in this case. Then, we have frozen the "octahedral parameters" in order to calibrate parameters related to the cubic slip systems. This last step is only based on the test results of the [111] oriented samples since the Schmid factors of the cubic systems are maximal for this orientation.

The calibration of the model parameters for each family of slip systems consists itself of three sub-steps. In the first one we have determined those parameters, which condition the short-range behavior. To this end we have simulated the cyclic tests and the beginning of the long-term relaxation, which mostly corresponds to the relaxation of the overstresses, $\tau_g^{overstress} \sim K_g \left(\dot{\gamma}_g^{vp}\right)^{1/n_g}$. Thereby we have identified the values of material parameters c_g, d_g, K_g and n_g. The static recovery (6) remained inactive during the first step. The second sub-step reduces to calibration of the static recovery term without softening. For this purpose we have used the stationary creep and the long-term relaxation results. In the final sub-step the full static recovery model including softening has been identified, where the parameter values determined in the previous sub-step have been used as starting values and where the full creep response as well as the long-term relaxation have been used.

The values of the plastic threshold L_{0g} (see (11)) have been identified by using the viscous relaxation results since L_{0g} influences the predicted viscoplastic overstress. It turned out that the plastic limit of the investigated material was reached at the temperatures of 600°C and 800°C, while it was never reached at 950°C and 1100°C. Therefore the value determined at 800°C has been assumed for L_{0g} at temperatures higher than 800°C.

4 Calibration Results

In what follows we present the results of the calibration procedure for the temperatures 800°C and 1100°C, since they are representative of the behavior of the superalloy in the whole temperature range of interest.

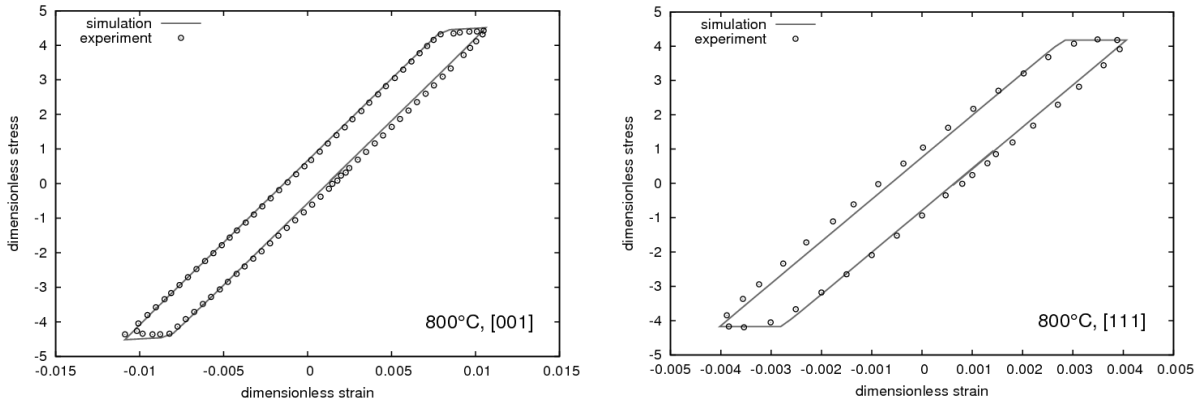

Figure 4: Predicted stress-strain hystereses against experimental data (open cycles) for the cyclic tests at 800°C along [001] (left) and [111] (right) crystallographic directions.

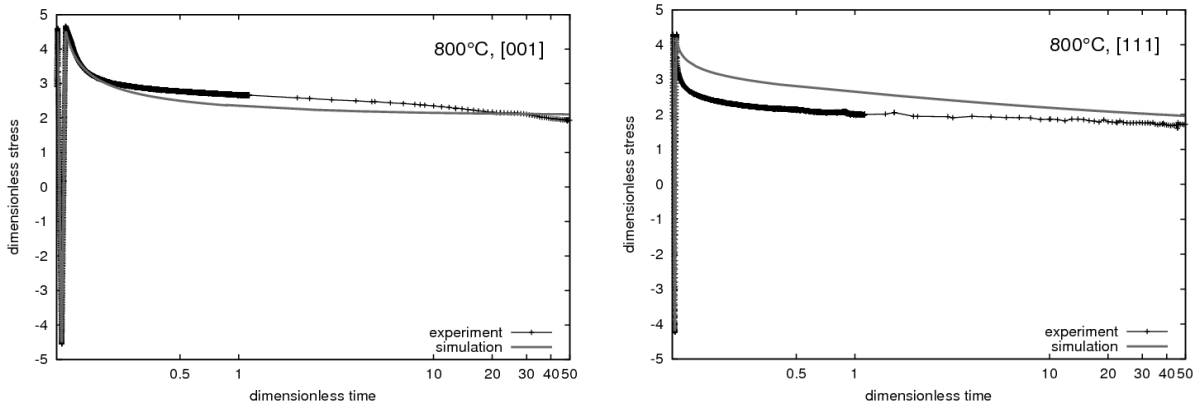

Figure 5: Predicted relaxation curves against experimental data. The tests were carried out at 800°C along [001] (left) and [111] (right) crystallographic directions.

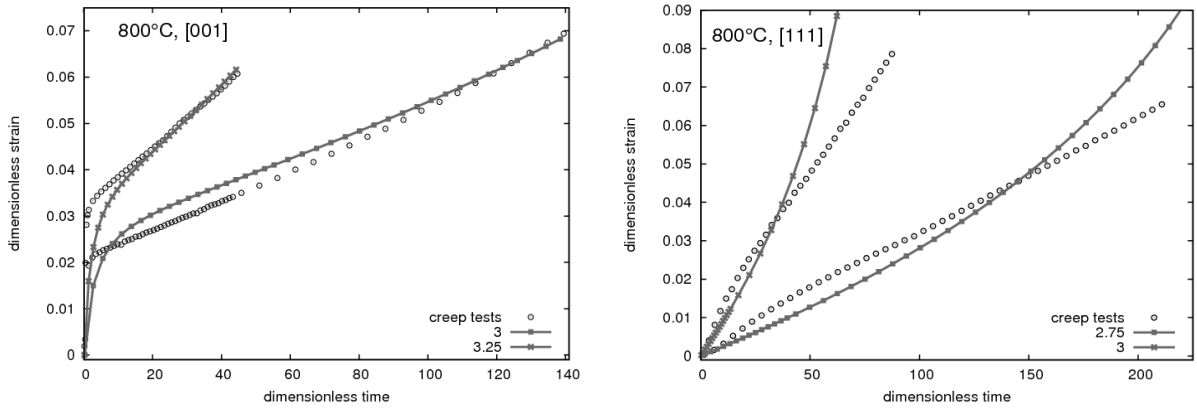

Figure 6: Predicted creep curves against experimental data (open cycles). The tests were carried out at 800°C along [001] (left) and [111] (right) crystallographic directions.

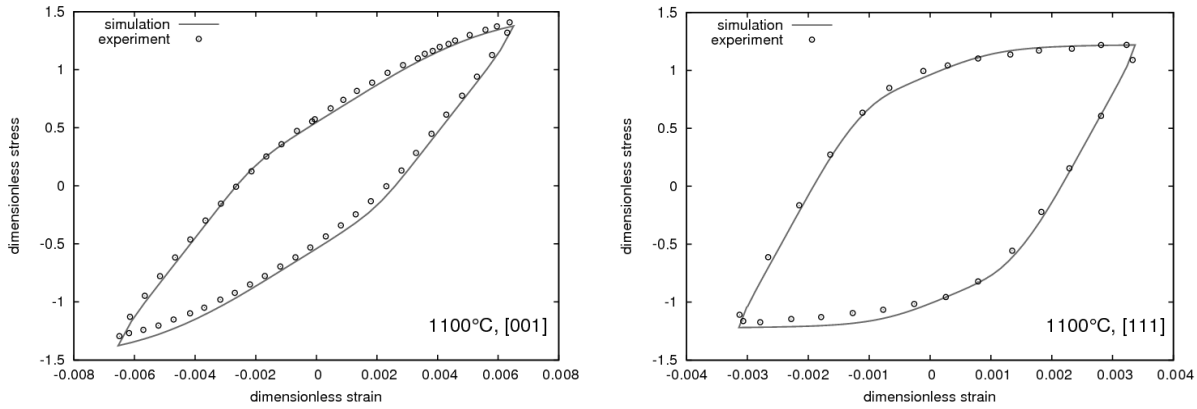

Figure 7: Predicted stress-strain hystereses against experimental data (open cycles) for the cyclic tests at 1100°C along [001] (left) and [111] (right) crystallographic directions.

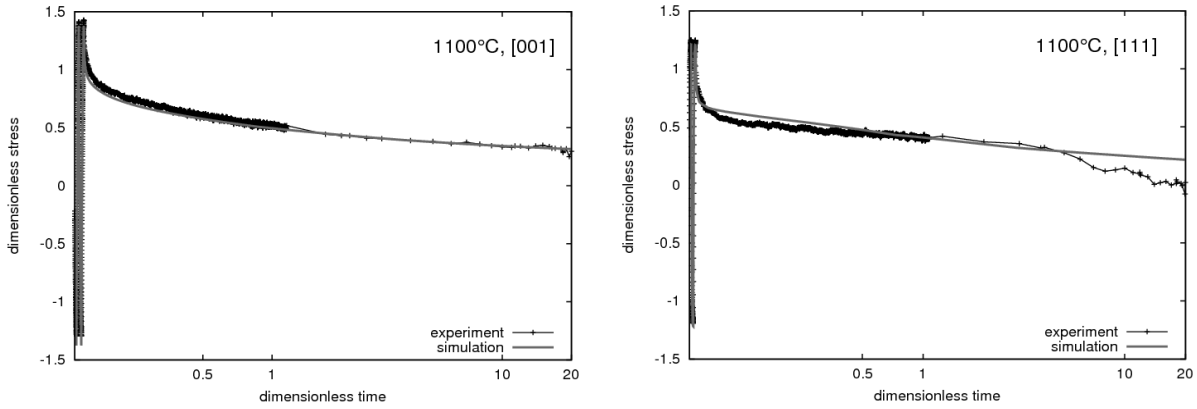

Figure 8: Predicted relaxation curves against experimental data. The tests were carried out at 1100°C along [001] (left) and [111] (right) crystallographic directions.

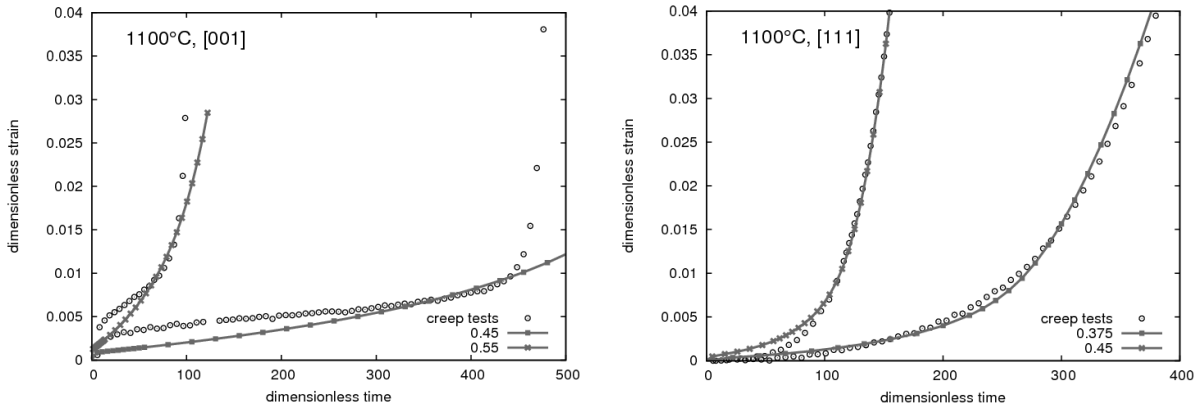

Figure 9: Predicted creep curves against experimental data (open cycles). The tests were carried out at 1100°C along [001] (left) and [111] (right) crystallographic directions.

5 Verification and Discussion

The model has been verified on the basis of the experimental data for the cyclic (Figure 10) and creep (Figure 11) tests along the [011] crystallographic direction and for the non-isothermal cyclic tests (Figures 12 and 13).

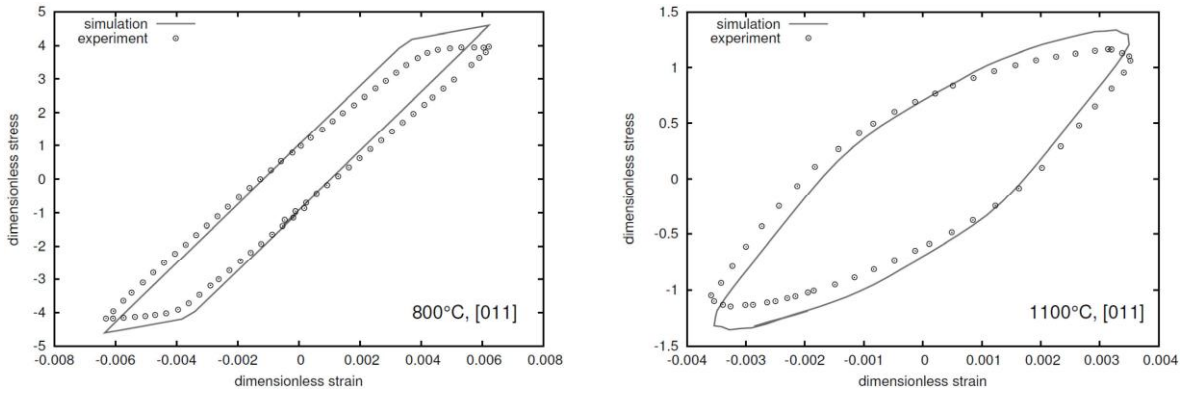

Figure 10: Predicted stress-strain hystereses against experimental data (open cycles) for the cyclic tests along [011] crystallographic direction at 800°C (left) and at 1100°C (right).

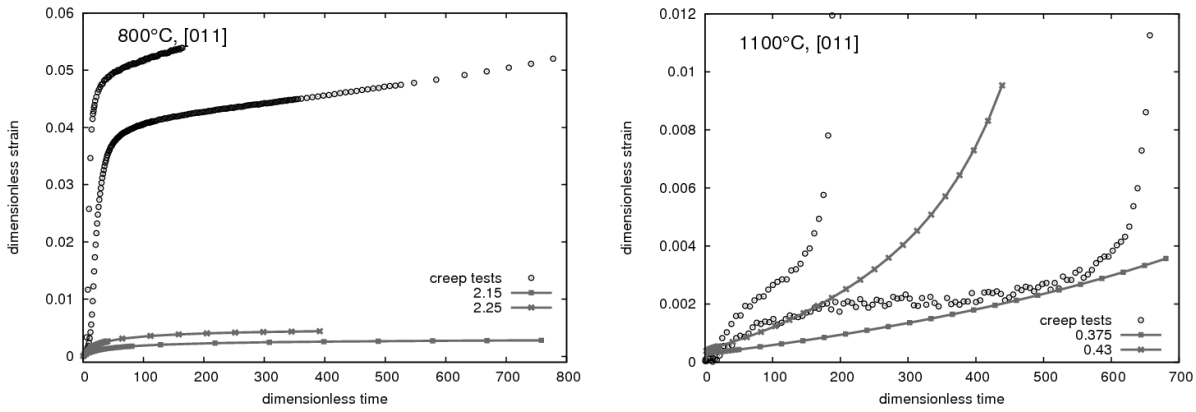

Figure 11: Predicted creep curves against experimental data (open cycles). The tests were carried out along [011] crystallographic direction at 800°C (left) and at 1100°C (right).

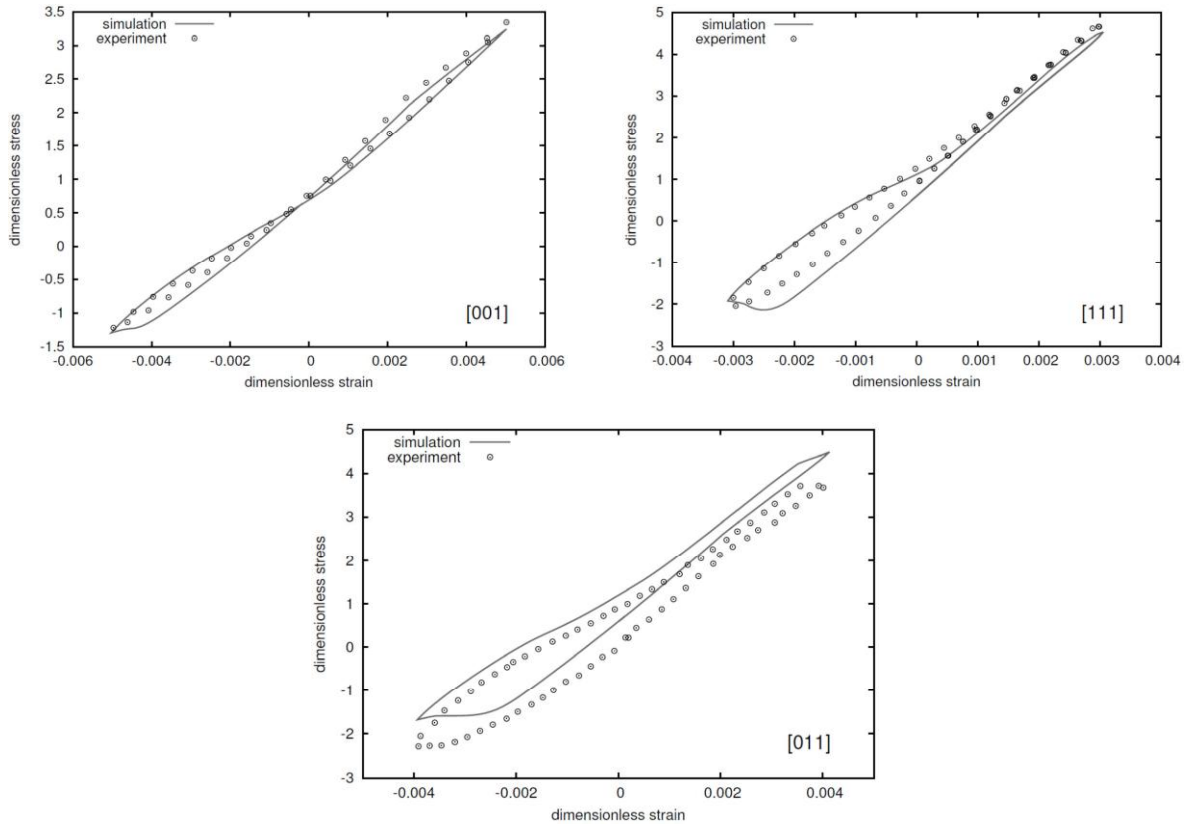

Figure 12: Predicted stress-strain hystereses against experimental data for 135° out of phase thermo mechanical fatigue tests in the temperature range from 600°C to 1100°C. The tests were carried out along [001] (left), [111] (right) and [011] (bottom) crystallographic directions.

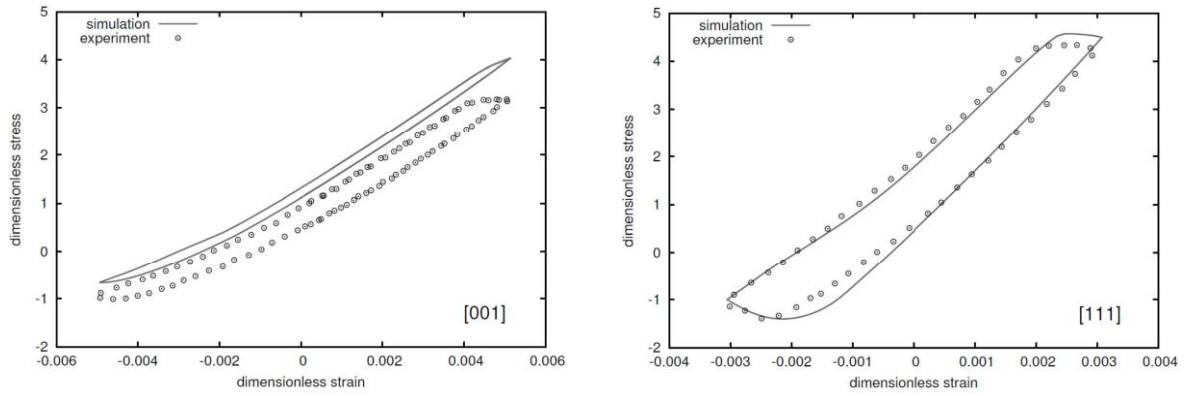

Figure 13: Predicted stress-strain hystereses against experimental data for 180° out of phase thermo mechanical fatigue tests at the temperature range from 600°C to 1100°C. The tests were carried out along [001] (left) and [111] (right) crystallographic directions.

The isothermal cyclic behavior in the [011] orientation as well as the non-isothermal cyclic behavior for all orientations are reasonably well described. However, the pronounced primary creep range in the [011] orientation at 800°C is largely underestimated. The origin of this discrepancy is clearly related to the activity of the {111}<112> slip systems, which have been reported to be predominant at 750°C (Chen and Knowles, 2003) and at 850°C (Sass, Glatzel et al., 1996) in the alloy CMSX-4. Indeed, some of the {111}<112> slip systems have higher Schmid factors in the [011] specimens than in the [001] and [111] specimens and numerous Superlattice Stacking Faults (SSF) have been observed in the γ' precipitates in crept specimens at both temperatures.

Note that there is no principal difficulty in incorporating these deformation mechanisms in the model by including additional slip systems. Indeed, cutting of γ' precipitates by Superlattice Intrinsic Stacking Faults was

already considered in a constitutive model by Fedelich (1999). However, for temperatures higher than 900°C, the octahedral and cubic slip systems become predominant. Hence, the three types of slip systems must be considered as competing over the whole temperature range, while the relative contribution of each type of slip system is strongly temperature dependent and extremely difficult to infer from the tests. Accordingly, if the three types of slip systems were considered simultaneously, the difficulty would just be transferred to the determination of the related model parameters. Indeed, on account of their Schmid factors, the "stacking fault systems" can be a priori active for all orientations [001], [111] and [011] so that the procedure described in section 3.4, which splits the identification of the parameters for each slip system, is no longer applicable. In regard of the large number of parameters, an unambiguous simultaneous determination of the parameters of the octahedral and the "stacking fault" systems is practically excluded. In conclusion, an improvement of creep modeling in [011] specimens at the moderate temperatures requires a deeper understanding of the kinetics and temperature dependence of the stacking faults mechanisms and possibly significant adaptations of the present model.

6 Conclusions

The current model noticeably improves the capability of the Cailletaud model to predict

- the relaxation behavior at all time scales,
- the softening-induced creep acceleration (beginning of tertiary creep),
- the rate-independent flow.

Also the non-isothermal behavior is reasonably simulated in the investigated temperature range 600°C – 1100°C.

The model has been calibrated by using isothermal test data from [001] and [111] specimens only. Non-isothermal tests and [011] specimens have been considered for verification. The agreement for the [011] oriented specimens is in general acceptable with the noticeable exception of creep at 800°C. According to the literature, the very high creep rates observed in [011] specimens at moderate temperatures 700°C – 800°C are due to the operation of additional deformation mechanisms known as Superlattice Intrinsic or/and Extrinsic Stacking Faults. The unambiguous identification of the relative contribution of theses slip systems for the whole temperature range is still an open issue.

Acknowledgments

The authors thank Dr G. Dhondt, Dr M. Becker and Dr E. Affeldt from the MTU Aero Engines for useful discussions. The research was supported by the Federal Ministry of Economics and Technology (Germany) under the LUFO-IV program.

References

Armstrong, P. J.; Frederick, C. O.: A mathematical representation of the multiaxial Bauschinger effect. *Materials at High Temperatures*, 24, (2007), 1-26.

Becker, M.; Hackenberg, H.-P.: A constitutive model for rate dependent and rate independent inelasticity. Application to IN718. *International Journal of Plasticity*, 27(4), (2011), 596-619.

Chaboche, J. L.: A review of some plasticity and viscoplasticity constitutive theories. *International Journal of Plasticity*, 24(10), (2008), 1642-1693.

Chen, Q. Z.; Knowles, D. M.: Mechanism of <1 1 2>/3 slip initiation and anisotropy of [gamma]' phase in CMSX-4 during creep at 750 °C and 750 MPa. *Materials Science and Engineering A*, 356(1-2), (2003), 352-367.

Fedelich, B.: A microstructure based constitutive model for the mechanical behavior at high temperatures of nickel-base single crystal superalloys. *Computational Materials Science*, 16(1-4), (1999), 248-258.

Glatzel, U.; Brehm, H.: Material model describing the orientation dependent creep behavior of single crystals based on dislocation densities of slip systems. *International Journal of Plasticity*, 15(3), (1999), 285-298.

Kindrachuk, V.; Fedelich, B.: Stress update algorithm for the combined viscoplastic and plastic behaviours of single-crystal superalloys. *International Journal for Numerical Methods in Engineering*, 88, (2011), 83-102.

Kindrachuk, V.; Fedelich, B., et al.: Simulation of mechanical behaviour in a single crystal nickel-basis superalloy at high temperature. Euro Superalloys, Wildbad Kreuth, (2010).

Li, S. X.; Smith, D. J.: Development of an anisotropic constitutive model for single-crystal superalloy for combined fatigue and creep loading. *International Journal of Mechanical Sciences*, 40(10), (1998), 937-948.

MacLachlan, D. W.; Wright, L. W., et al.: Constitutive modelling of anisotropic creep deformation in single crystal blade alloys SRR99 and CMSX-4. *International Journal of Plasticity*, 17(4), (2001), 441-467.

Meric, L.; Poubanne, P., et al.: Single Crystal Modeling for Structural Calculations: Part 1 - Model Presentation. *Journal of Engineering Materials and Technology*, 113(1), (1991), 162-170.

Sass, V.; Glatzel, U., et al.: Anisotropic creep properties of the nickel-base superalloy CMSX-4. *Acta Materialia*, 44(5), (1996), 1967-1977.

Simo, J. C.; Hughes, T. J. R.: *Computational Inelasticity*. New York, Springer Verlag (1998).

Staroselsky, A.;Cassenti, B. N.: Creep, plasticity, and fatigue of single crystal superalloy. *International Journal of Solids and Structures*, 48(13), (2011), 2060-2075.

Address: Dr. Bernard Fedelich and Dr. Vitaliy Kindrachuk, BAM Federal Institute for Materials Research and Testing, Div 5.2 Mechanical Behaviour of Materials, D-12205 Berlin, Germany.
email: bernard.fedelich@bam.de; vitaliy.kindrachuk@bam.de.